High shear enrichment improves the performance of the anodophilic microbial consortium in a microbial fuel cell

Hai The Pham,[1] Nico Boon,[1] Peter Aelterman,[1]
Peter Clauwaert,[1] Liesje De Schamphelaire,[1]
Patrick van Oostveldt,[2] Kim Verbeken,[3]
Korneel Rabaey[4] and Willy Verstraete[1]*
[1]*Laboratory of Microbial Ecology and Technology (LabMET), Ghent University, Coupure Links 653, B 9000 Ghent, Belgium.*
[2]*Department of Molecular Biotechnology, Ghent University, Coupure Links 653, B 9000 Ghent, Belgium.*
[3]*Department of Metallurgy and Materials Science, Ghent University, Technology park 903, 9052 Zwijnaarde, Belgium.*
[4]*Advanced Water Management Centre, University of Queensland, Brisbane, QLD 4072, Australia.*

Summary

In many microbial bioreactors, high shear rates result in strong attachment of microbes and dense biofilms. In this study, high shear rates were applied to enrich an anodophilic microbial consortium in a microbial fuel cell (MFC). Enrichment at a shear rate of about 120 s^{-1} resulted in the production of a current and power output two to three times higher than those in the case of low shear rates (around 0.3 s^{-1}). Biomass and biofilm analyses showed that the anodic biofilm from the MFC enriched under high shear rate conditions, in comparison with that under low shear rate conditions, had a doubled average thickness and the biomass density increased with a factor 5. The microbial community of the former, as analysed by DGGE, was significantly different from that of the latter. The results showed that enrichment by applying high shear rates in an MFC can result in a specific electrochemically active biofilm that is thicker and denser and attaches better, and hence has a better performance.

Introduction

Microbial fuel cells (MFCs) employ microorganisms as biocatalysts to convert chemical energy comprised in electron donors to electrical energy (Allen and Bennetto, 1993; Logan *et al.*, 2006). Due to their unique characteristics, MFCs are considered to have potential applications in the domains of power supply (Wilkinson, 2000; Aelterman *et al.*, 2006; Biffinger *et al.*, 2007), biological oxygen demand sensors (Chang *et al.*, 2006) and especially in sustainable wastewater treatment (Rabaey and Verstraete, 2005). However, to make these applications of MFCs feasible, a number of limitations need to be overcome (Aelterman *et al.*, 2006; Pham *et al.*, 2006). Most researchers thus far have been focusing on the activity of the biocatalysts, electron transfer losses both at the anodes and the cathodes, and the internal resistance (Logan *et al.*, 2006). The electron transfer between the bacterial catalysts and the anodic electrode poses a serious challenge.

Attempts have been made to understand the mechanisms of the anodic electron transfer of an MFC. To date, the proposed mechanisms include: (i) direct electron transfer either by membrane-associated cytochromes (Kim *et al.*, 1999; Bond and Lovley, 2003) or conductive pili or pilus-like appendages (Reguera *et al.*, 2005; Gorby *et al.*, 2006) and (ii) the mobile redox mediator-associated electron transfer (Rabaey and Verstraete, 2005; Marsili *et al.*, 2008). In addition, recently, the interactions between bacteria have been shown to play an important role in the anodic electron transfer of, e.g. a Gram-positive bacterium dominant in the microbial community of an acetate-fed MFC (Rabaey *et al.*, 2007; Pham *et al.*, 2008). Nevertheless, from the existing concepts, a strategy to improve the electron transfer with an order of magnitude is still needed.

The anodic microbial consortium of an MFC grows in biofilm structures (Kim *et al.*, 2004; Rabaey and Verstraete, 2005; Reguera *et al.*, 2006). Studies on the composition of such microbial communities have been carried out but no work has been related to the engineering of the MFC biofilm structure in order to improve the performance of the MFC. It has been reported that high shear rates (below the level called tensile strength) result in stronger aggregation and attachment of microbes (with biomass densities up to 70 g l^{-1}) and hence more compact (denser) biofilms in many microbial systems, such as in nitrifying reactors, fluidized bed reactors or airlift suspension

reactors etc. (Kugaprasatham *et al.*, 1992; Kwok *et al.*, 1998; Dunsmore *et al.*, 2002; van Loosdrecht *et al.*, 2002). Therefore, in this study, we investigated the influence of high shear rates on the establishment and the structuring as well as the performance of a microbial community in the anode of an MFC. We examined whether this can be applied as a biofilm-modifying approach to improve the anodic electron transfer and thus the overall performance of MFCs.

Results

Effect of shear rate on the electricity generation and enrichment of the electroactive microbial consortium in an MFC

With a shear rate starting from an estimated level of 80 s^{-1} for 5 days and increasing every 2 days, the average current generated by the treated MFC increased concomitantly with the increased shear rates up to an estimated level of 120 s^{-1} (Fig. 1). Above that level, the current started to decrease (Fig. 1A). The total DNA amount of the bacterial cells attached to the electrode changed in a similar pattern (Fig. 1A). The 'optimal shear rate' for enrichment was thus determined to be approximately 120 s^{-1}. The MFC was subsequently operated under the condition at which the estimated shear rate was 120 s^{-1} for 2 weeks to complete the enrichment, before it was operated in default operational mode. Typical current patterns from one of three repeated operations in such a way were shown in Fig. 1B. During the shear stress period, the MFC generated a current of 5.6 ± 0.6 mA versus 2.1 ± 0.2 mA for the control (the low shear enriched MFC) (Fig. 1B). When the high shear stress stopped, the current initially dropped but quickly recovered and subsequently increased to 7.2 ± 0.8 mA (Fig. 1B). The current generated by the high shear enriched MFC at plateau state after the enrichment period reached average values of 6.0 ± 0.5 mA, which is about three times higher than that generated by the low shear enriched MFC (2.0 ± 0.3 mA). Indeed, at plateau state, the high shear enriched MFC could produce a maximum current of 8.1 ± 1.1 mA and a maximum power density of about 160 W m^{-3} while the low shear enriched MFC could maximally produce 3.0 ± 0.3 mA and about 50 W m^{-3} (Fig. 2). The chemical oxygen demand (COD) removal efficiency of the high shear enriched MFC was 24 ± 2% and that of the low shear enriched MFC was 20 ± 4%. Using these values and Eq. V, the electron efficiency of the former was calculated to be 25 ± 2% and that of the latter was 10 ± 2%.

Microbiological analysis of the microbial consortia

After the enrichment period, when the current generation was stable, the microbial consortia of the high shear
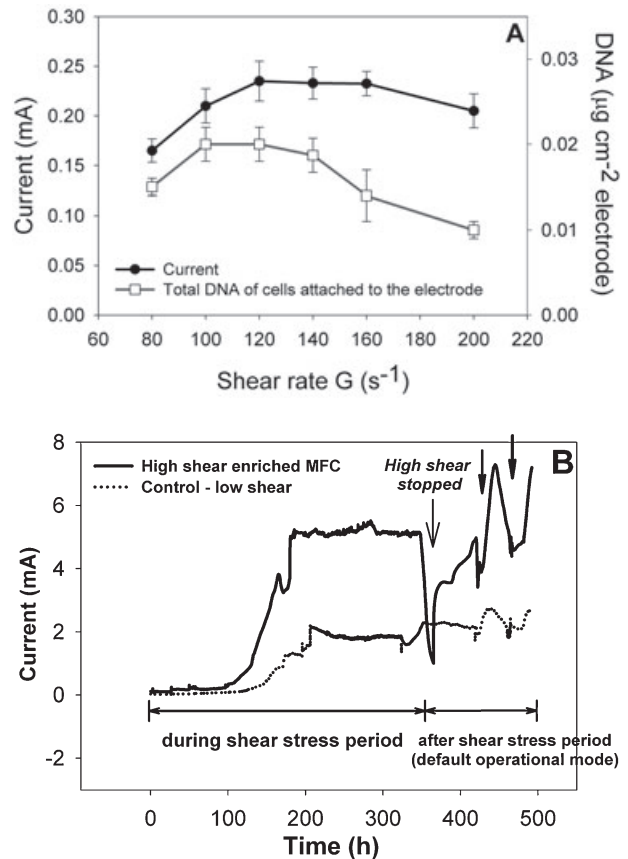

Fig. 1. A. Determination of the 'optimal shear rate' for the high shear rate enrichment.
B. The current patterns during and after the enrichment period of the high shear enriched MFC and the control (the low shear enriched MFC). Bold-lined arrows indicate the moments when the catholyte was replenished (for both MFCs). The external resistance of each MFC was 20 ohm. Default operational mode: the MFCs were fed at a flow rate of 0.5 ml min^{-1} (14.4 g COD day^{-1} l^{-1} net anodic capacity).
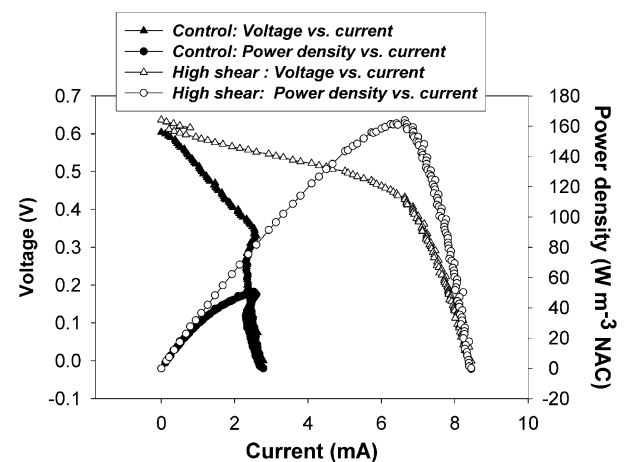

Fig. 2. Polarization curves of the MFCs at the plateau state of electricity generation (500 h after the enrichment).

Table 1. ATP amount, DNA amount and biomass density of the anodic biofilm enriched at high shear rates in comparison with those under low shear.

	ATP (pmol cm⁻² electrode)	DNA (µg cm⁻² electrode)	Biomass density (estimated from DNA amount)	mg ATP/g biomass (VSS)
High shear enriched MFC (open circuit)	60 ± 7	0.25 ± 0.02	0.127 mg VSS cm⁻² electrode surface Or: 122 mg VSS cm⁻³ biofilm	0.27
Low shear enriched MFC (control)	18.6 ± 2	0.05 ± 0.007	0.026 mg VSS cm⁻² electrode surface Or: 61 mg VSS cm⁻³ biofilm	0.41
High shear enriched MFC (open circuit)	9 ± 2	0.05 ± 0.007	0.01 mg VSS cm⁻² electrode surface	0.52
Planktonic cells[a] (non-MFC conditions, no shear)	100 ± 12	0.3 ± 0.02	0.153 mg VSS	1.25

a. The cell suspension of the planktonic cells had the same cell density (OD = *ca* 0.250) as that of the cells harvested from the electrode of the high shear enriched MFC.
For reference, the mg ATP/g VSS ratio ranges from 0.25 to 1.67 for activated sludge (Kucnerowicz and Verstraete, 1979)

enriched MFC and the low shear enriched MFC were analysed with respect to ATP content, total DNA (Table 1) and biofilm configuration. The ATP content of the bacteria of the high shear enriched MFC was 60.0 ± 7.0 pmol cm⁻² electrode, three times higher compared with 18.6 ± 2.0 pmol cm⁻² electrode of the low shear enriched MFC (Table 1). Total DNA of the bacteria from the high shear enriched MFC (0.25 ± 0.02 µg cm⁻² electrode) was five times higher than that of the low shear enriched MFC (0.05 ± 0.007 µg cm⁻² electrode) (Table 1). Taking the ratio of 1.96 mg DNA g⁻¹ biomass (volatile suspended solid, VSS) (Kim *et al.*, 2008), the corresponding biomass density was about 0.127 ± 0.012 mg VSS cm⁻² electrode surface for the high shear enriched MFC and 0.026 ± 0.003 mg VSS cm⁻² electrode surface for the low shear enriched. Confocal laser scanning microscopy (CLSM) observation (Fig. 3B) showed that right after enrichment, the biofilm on the electrode surface of the high shear enriched MFC had a relatively smooth surface and it was already thicker than the biofilm of the low shear enriched MFC. The average and maximum thickness values of the biofilm of the high shear enriched MFC right after enrichment, as calculated by COMSTAT (Table 2), were about 11 and 55.7 µm respectively, while those of the low shear enriched were about 4.15 and 8 µm respectively. After 2 months, the biofilm of the high shear enriched MFC became very heterogeneous with irregular thickness (Fig. 3C), but the average and maximum thickness values remained approximately the same: 10.4 and 58 µm respectively. The biofilm of the low shear enriched MFC was relatively homogenous with a regular thickness (Fig. 3A). From the average thickness values, the biomass densities of the high shear enriched MFC right after enrichment and the low shear enriched MFC were calculated to be about 122 and 61 mg VSS cm⁻³ biofilm respectively. These results suggested that the biofilm of the high shear enriched MFC is not only thicker but also denser than that of the low shear enriched MFC.

Scanning electron microscopy observation

The electrode surface of the high shear enriched MFC and the low shear enriched MFC after 2 months of operation were observed with scanning electron microscopy (SEM) (Fig. 4). In comparison with that of the low shear enriched MFC, the electrode surface of the high shear enriched MFC was covered much more densely with bacterial cells, which corroborates the earlier findings with CLSM. In addition, in the case of the low shear enriched MFC, bacteria were distributed unevenly on the electrode surface, which was not the case for the high shear enriched MFC.

Microbial community analysis

The DGGE and sequencing analysis of the bacterial communities showed that the anodic microbial community of the high shear enriched MFC was very different from that of the low shear enriched MFC (Fig. 5), although both had some abundantly present species in common: *Phyllobacterium* and *Pseudomonas* sp. (corresponding to bands 6 and 7). Some species (corresponding to bands 1, 8–11, especially) were only dominant in the community of the high shear enriched MFC, not in the community of the low shear enriched MFC and vice versa. Interestingly, most of characteristic dominant species of the community of the high shear enriched MFC only showed very low sequence homology (< 96%) even though the sequence length was short (200 bp). On the contrary, most of dominant species of the community of the low shear enriched MFC could be determined as known bacteria (with BLAST sequence homology > 96%).

Discussion

The increasing high shear rates initially resulted in an increase of the current and the total DNA amount of the bacterial cells attached to the electrode but, above the
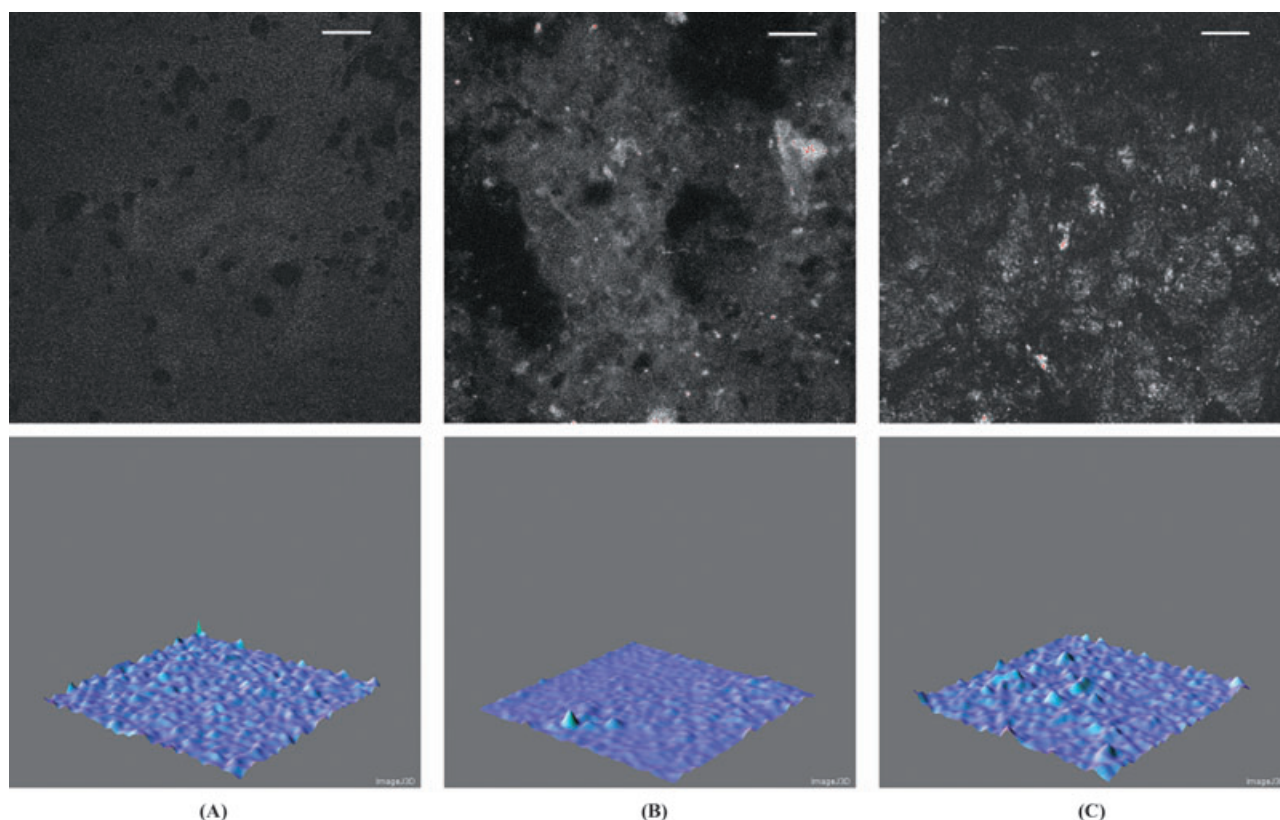
Fig. 3. CLSM images of the biofilms fixed with methanol and dyed with propidium iodine on the electrodes of the low shear enriched MFC (A), the high shear enriched MFC right after the enrichment (B) and the high shear enriched MFC 2 months after the enrichment (C). Top images: total fluorescent signals (bars, 18 μm); bottom images: 3D surface plots developed from the fluorescent signals using ImageJ software. The biofilm analysis was done with COMSTAT software (see Table 2).

estimated shear rate of 120 s^{-1}, both the current and the DNA amount decreased (Fig. 1A). This demonstrated cell detachment at shear rates higher than that level. Our hypothesis is that up to that maximum level, bacteria attach to the electrode, thereby transferring electrons by more mechanisms such as via direct contacts (outer membrane proteins or nanowires), in addition to using only redox mediators. We therefore applied the shear rate of approximately 120 s^{-1} for the enrichment process and further studied the enriched anodic microbial consortium. It is clear that after the enrichment period, when operated in the same continuous mode (at the same shear rate) as the low shear enriched MFC, the high shear enriched

MFC still maintained the higher current and power output (Fig. 1). This eliminates the possibilities that fast pH changes or high diffusivity of nutrients (high mass transfer) caused by high flow rates, rather than the high shear rates, indeed resulted in the increase of electricity generation. One should notice the initial drop of the current of the high shear enriched MFC after the enrichment period. As the current was subsequently recovered very quickly before becoming stable at the high levels, this drop reflects that the microbial community is quite sensitive to disturbances. In this case, the stop of the high shear was obviously a dramatic shift of environmental conditions that disturbed the microbial community. However, it is evident

Table 2. Structure analysis (using COMSTAT software) of the anodic biofilms observed by CLSM, as described in Fig. 3.

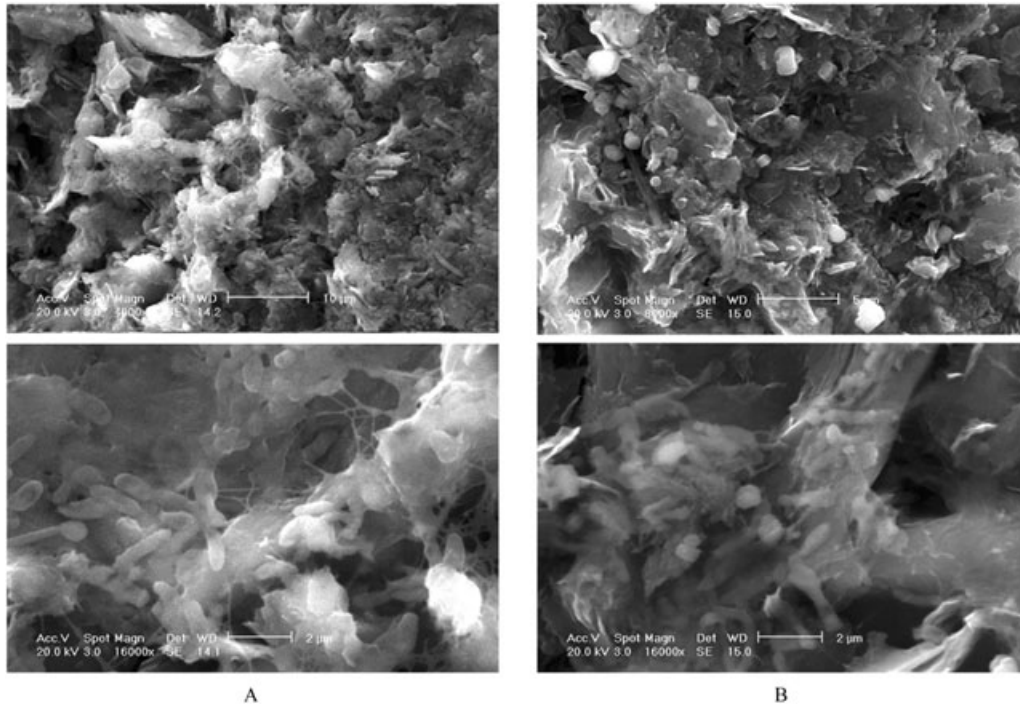| Parameter	Low shear enriched MFC	High shear enriched MFC (right after enrichment)	High shear enriched MFC (2 months after enrichment)
Total biomass (μm^3/μm^2)	0.73	1.52	1.22
Average thickness (μm)	4.15	11.13	10.40
Surface to biovolume ratio (μm^2/μm^3)	7.32	4.86	6.76
Maximum thickness (μm)	8.16	55.68	58.08

Fig. 4. SEM images.
A. The electrode surface of the high shear enriched MFC at magnification levels of 4000× (top) and 16000× (bottom).
B. The electrode surface of the low shear enriched MFC at magnification levels of 8000× (top) and 16000× (bottom).

that the microbial community could rapidly recover and readjust to a new set of environmental conditions.

Microbiological analyses revealed differences between the anodic biofilms of the two MFCs. Both biomass comparison (through ATP and DNA measurement) and biofilm analysis based on CLSM observations showed that the bacterial density on the electrode surface of the high shear enriched MFC was substantially higher than that of the low shear MFC. This suggests that the biofilm formed under high shear rates is denser and thicker,
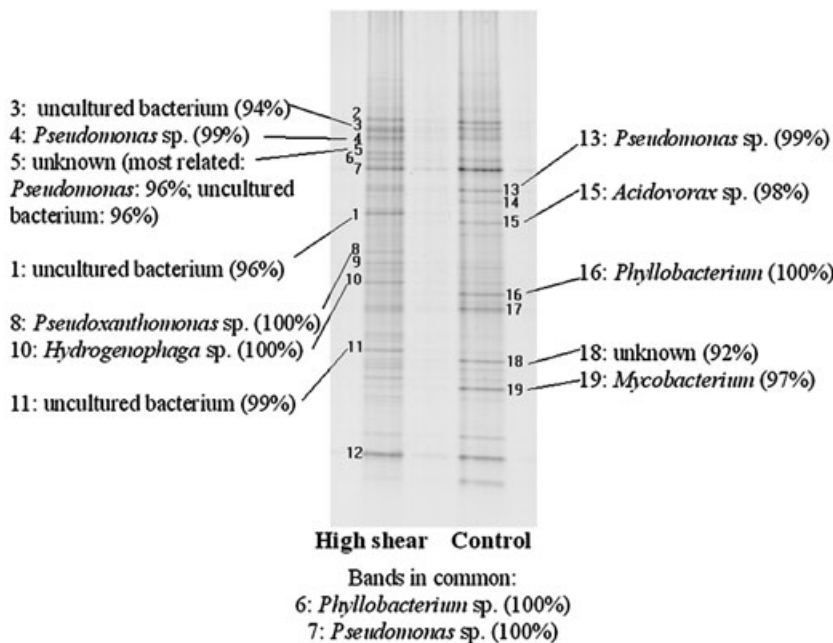

3: uncultured bacterium (94%)
4: *Pseudomonas* sp. (99%)
5: unknown (most related:
Pseudomonas: 96%; uncultured
bacterium: 96%)

1: uncultured bacterium (96%)

8: *Pseudoxanthomonas* sp. (100%)
10: *Hydrogenophaga* sp. (100%)

11: uncultured bacterium (99%)

13: *Pseudomonas* sp. (99%)

15: *Acidovorax* sp. (98%)

16: *Phyllobacterium* (100%)

18: unknown (92%)
19: *Mycobacterium* (97%)

High shear   Control

Bands in common:
6: *Phyllobacterium* sp. (100%)
7: *Pseudomonas* sp. (100%)

Fig. 5. DGGE analysis of the anodic microbial communities in the high shear enriched MFC (High shear) and the low shear enriched MFC (Control) and BLAST analysis results of the DGGE fragment sequences of the major species of the two communities. The DGGE was repeated three times with three samples collected from three different anodic electrode graphite plates of each reactor. As the results of these repetitions were absolutely similar, only typical patterns were shown here. Percentage numbers indicate the highest corresponding levels of homology of the sequences in comparison with sequences in the Genebank database.

which is most probably the reason for the higher electricity generation. Such a thicker and denser biofilm could not only improve the electron transfer via direct contacts, but also enhance the electron transfer via electron shuttles as more cells might be involved in electron transfer and more shuttles could be produced. It is interesting to note that the amount of ATP present in the biofilm of the MFC enriched at high shear rates was higher than that by the biofilm of the control, but the mg ATP/g biomass ratio of the former was lower than that of the latter and much lower than that of the planktonic cells (Table 1). A determination of the ATP level is the measurement of the energy that bacteria produce and use for their own metabolism. Possibly in this case, due to higher metabolic turnover rates, as evidenced by the higher current generation, bacteria in the MFC enriched at high shear rates obtain less ATP to maintain themselves.

The SEM observations also indicated a denser colonization on the electrode of the high shear enriched MFC. To date, many studies have shown that high shear rates result in stronger aggregation and denser biofilms with concomitant improved performance (Kugaprasatham *et al.*, 1992; Kwok *et al.*, 1998; Dunsmore *et al.*, 2002; van Loosdrecht *et al.*, 2002). However, there is a limiting level called tensile strength at which too high a shear rate causes detachment of the biofilm (Ohashi and Harada, 1996; Picioreanu *et al.*, 2001). In this research, the 'critical' G value around $120 \, s^{-1}$ is possibly corresponding to this tensile strength.

According to van Loosdrecht and colleagues (2002), the higher the shear rate is, the less morphologically heterogeneous the biofilm should be, although the cell density can be higher. In our study, the electroactive biofilm formed under high shear was relatively homogenous (i.e. it had a smooth surface) right after enrichment. This is consistent with the aforementioned principle. After 2 months of further operation under low shear conditions, the high shear enriched biofilm became heterogeneous. This heterogeneity of the biofilm at that time was possibly the result of the post-enrichment 'docking' of bacteria onto the biofilm base initially formed.

The community analysis results (DGGE) (Fig. 5) clearly showed that the bacterial compositions of the communities of the high shear enriched MFC and the low shear enriched MFC are significantly different. It might be also interesting to investigate the archaeal compositions of the two communities. However, as most of electrochemically active bacteria known thus far are eubacteria (Logan and Regan, 2006), in this study we only focus on the eubacterial compositions of the two communities. Indeed, the fact that their eubacterial compositions were largely different already suggested that the two whole communities were different. From the

results, it is not possible to affirm which specific bacteria are responsible for the differences in performance of the high shear enriched MFC and the low shear enriched MFC. However, the results suggest that enrichment at low shear could involve 'normal' bacteria to take over the anodic electron transfer whereas applying high shear rates (an extreme condition) appears to select for special bacteria (thus far not identified) that are not favoured under normal conditions. It has been reported that a turbulent environment (under high shear) resulted in the dominance of bacteria that were not dominant in reactors operated under normal shear rate (Cao and Alaerts, 1995). Similar phenomena have been reported for activated sludge processes (Houtmeyers *et al.*, 1980). In this study, as most of the bacteria in the MFC enriched with high shear rates are not yet identified, it is difficult to postulate how the anodic biofilm formed under high shear conditions functions to improve the electricity generation. However, this result strongly suggests that the biofilm consists of the bacteria that are rather specific for high shear enrichment conditions.

In summary, combining all the results, it is postulated that enrichment under high shear rates in an MFC can result in modification of an electrochemically active biofilm that is thicker and denser and hence can transfer electrons more efficiently. One of the main bottlenecks of this approach is that to apply it, the flatness of electrode surface is of crucial importance. Yet this contradicts with the aim to have large contact surfaces. One may notice that the power output and electron efficiency of the reactor type used in this study is relatively low compared with those by other systems. For example, the stack type MFC, which was also operated under normal low shear, has previously yielded power densities of about $250 \, W \, m^{-3}$ net anodic capacity (NAC) (Aelterman *et al.*, 2006), while the low shear enriched MFC in this research could only produce about $50 \, W \, m^{-3}$ NAC (Fig. 2). This is likely due to the much smaller electrode surfaces used in this study that increases the activation overpotential effects, in addition to diffusion limitations. However, it should be noticed that the high shear enriched MFC in this study could reach about $160 \, W \, m^{-3}$ NAC (Fig. 2). Approaches should be worked out to compromise the criterion of large electrode surface and imposition of shear on the surface, at least during the preparation of the anodic biofilm.

The results of this research strongly suggest that high shear enrichment can be used as a strategy to obtain better performing anodic MFC microbial consortia. Also, the application of this approach for the improvement of biocathodes deserves attention in further studies. The strategy can be integrated in the optimization of MFC configurations in the future.
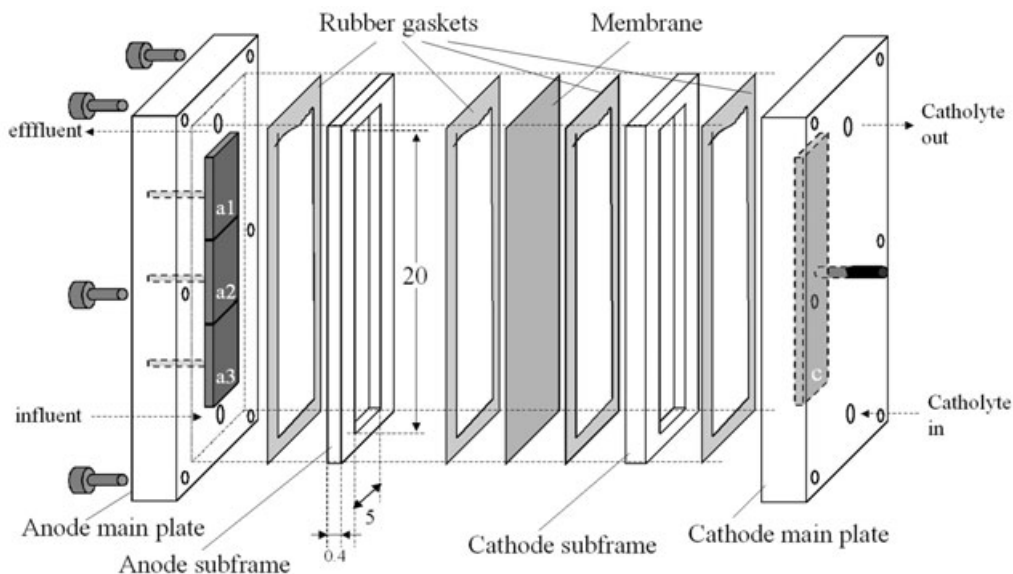
Fig. 6. Scheme of the reactor designed in this study. a1, a2, a3: anodic electrode graphite plates (each connected to a graphite rod that is connected with wires to others and to a shared external circuit and data acquisition system); c: cathodic electrode graphite plate (surrounded with graphite granules). Numbers indicate the dimensions (in cm) of the anode working space.

Experimental procedures

Reactor design

The MFC reactor design was based on the stack type MFC model (Aelterman *et al.*, 2006) in order to render the application of high shear rates feasible (Fig. 6). Perspex frames were used to construct the anode and cathode compartments, which were separated by a cation-specific membrane (Ultrex CMI7000, Membranes International, US). Each compartment included a main plate and a rectangle-holed frame (23 cm × 8 cm × 0.4 cm). On the main plate of the anode compartment, there were two larger holes (1 cm diameter) for the inlet and outlet of liquid (anolyte or catholyte) and three small holes through which three graphite rods (5-mm diameter each, Morgan, Belgium) penetrated to contact three graphite plates (Le Carbone, Belgium) functioning as the anodic electrodes. Each electrode plate had a 5 cm × 5 cm × 0.3 cm dimension and its surface was polished carefully using sand paper. The side of the electrode facing the main Perspex plate was glued to the plate and the other sides were covered with silicone (low conductivity) so that only the 5 cm × 5 cm side facing the membrane could be active when the MFC was operated. The anodic working space was 20 cm long (from top to bottom), 5 cm wide and 0.4 cm thin (Fig. 6). The cathode working space had a 20 cm × 5 cm × 1 cm dimension, containing graphite granules (diameters between 1.5 and 5 mm, Le Carbone, Belgium). On the cathode main plate, there were also two holes (1 cm diameter) for the inlet and outlet of the catholyte and one hole for the penetration of a graphite rod in contact with a graphite plate surrounded by the granules. To prevent leakage, rubber gaskets were placed between the Perspex parts when the reactor was assembled. The three anodic graphite rods and the three cathodic graphite rods were

connected through wires to a shared external circuit and to the data acquisition system.

Operational conditions

The reactor was operated at room temperature (22 ± 3°C). A sterile synthetic medium containing 0.75–1.00 g l^{-1} sodium acetate (0.58–0.78 g COD l^{-1}) prepared as previously described (Rabaey *et al.*, 2005) was used as the anode influent. The reactor was fed with the medium in continuous mode at a flow rate of 0.5 ml min^{-1} (corresponding to a low estimated shear rate of 0.3 s^{-1}) with a COD loading rate of approximately 0.72 g COD day^{-1} or 14.4 g COD day^{-1} l^{-1} net anodic capacity (default operational mode). The external resistance was 20 ohm. The catholyte was an aqueous solution of 50 mM $K_3Fe(CN)_6$ and 100 mM KH_2PO_4 buffer (Merck, Belgium) adjusted to pH 7 with 1 M NaOH. It was recirculated through the cathode matrix and replenished before its decolouration (Aelterman *et al.*, 2006).

For the enrichment of the electroactive bacteria in the anode, the inoculum was a mixture of an anaerobic sludge (from a wastewater treatment plant, DRANCO, Belgium), a soil sample (Coupure Links, Ghent, Belgium) and an effluent sample from an MFC fed with acetate (Aelterman *et al.*, 2006). This inoculum was initially mixed with the medium; the resulting mixture was recirculated through the anode compartment of the reactor using a tubal recirculation loop that had a negligible total capacity (approximately 3 ml) and was connected to the anode inlet and the anode outlet (Aelterman *et al.*, 2008), while the reactor was still fed continuously. To determine an 'optimal shear rate' for enrichment, a series of increasing recirculation rates were tested as follows: at the beginning, a recirculation rate of 2 ml s^{-1} was applied for 5 days; starting from day 6, the recirculation rate was increased

every 2 days, in an ascending order, from 2 to 2.5, 3, 3.5, 4 and 5 ml s^{-1} (corresponding to the increase of estimated shear rates from 80 to 100, 120, 140, 160 and 200 s^{-1}). During the tests, the changes of the current generation were followed and the total DNA of the bacterial cells attached to the electrode was measured. The 'optimal shear rate' is the shear rate at which we hypothesized that well-attaching electro-active bacteria start to attach to the electrode if the shear is decreased, starting from a very high level; if the shear is increased to a level higher than that shear rate, the bacteria detach from the electrode. All experiments to determine the 'optimal shear rate' were performed in triplicate. For the enrichment, the MFC was subsequently operated under the determined shear rate for 2 weeks.

After the enrichment, the recirculation was stopped and the reactor was operated in the default operational mode.

An identical MFC reactor was used as the control. It was seeded with the same inoculum and operated in the default operational mode from the beginning (enriched under low shear conditions). Except for the high shear treatment in the enrichment period, exactly the same treatments (catholyte changes, medium replenishments etc.) were applied for both the abovementioned reactor and the control.

For some measurements, suspensions of planktonic cells were prepared by cultivating the same inoculum in the same medium in shaken test tubes at 25°C.

The whole enrichment and post-enrichment experiments were repeated three times.

Calculation

The shear rate was estimated from the flow/recirculation rate as follows:

As the medium fed to the MFCs contained mostly water, it can be considered as a Newtonian fluid. As it is almost impossible to calculate the exact velocity gradient of the liquid moving in the anodic working space, we only could estimate shear rates assuming that this velocity gradient is uniform. According to the simplified rule applied for Newtonian fluid, the shear rate at the surface of the electrode G could be estimated as: G = v/d (Eq. 1) (Massey, 1983)

whereas v: velocity of the liquid movement; d: the distance from the centre layer of the moving liquid to the electrode surface (d, at millimeter level, can be considered to be the same for the whole surface of the electrode as the heterogeneity of the biofilm covering the electrode or the electrode surface itself is at micrometer level.)

v and d can be calculated as follows:

v = Q/S with Q being the flow/recirculation rate and S being the cross section (Eq. 2). Here only the path between the electrodes and the membrane could be counted, so S = the width of the anodic working space × (the thickness of the anodic working space – the thickness of the electrode) = 5 cm × (0.4 cm – 0.3 cm) = 0.5 cm^2 (Eq. 3).

d = the distance between the membrane and the electrode/ 2 = (the thickness of the anodic working space – the thickness of the electrode)/2 = (0.4 cm – 0.3 cm)/2 = 0.05 cm (Eq. 4)

Combining (1), (2), (3), (4), the recirculation rates of 2, 2.5, 3, 3.5, 4 and 5 ml s^{-1} were calculated to correspond to estimated shear rates of 80, 100, 120, 140, 160 and 200 s^{-1}.

Similarly, the feeding flow rate of 0.5 ml min^{-1} is corresponding to an estimated shear rate of 0.3 s^{-1}.

The NAC (the volume of liquid in the anode compartment) (Clauwaert *et al.*, 2007) was calculated as: NAC = the total volume of the anodic working space – the volume of the inserted electrodes = 20 cm × 5 cm × 0.4 cm – 5 cm × 5 cm × 0.3 cm × 3 = 17.5 cm^3 = 0.0175 l.

Electron efficiency (EE) was calculated as: EE = average obtained current I_{aver}/maximum attainable current $I_{max.at}$ (Eq. 5). $I_{max.at}$ (A or C/s) can be calculated from COD removal rate, as COD can be converted to charge Q (C). The relation between Q and COD is expressed as Q = 96 485 (C mol^{-1} electrons) × COD (g)/32 (g mol^{-1} O$_2$) × 4 mol electrons mol^{-1} O$_2$. COD removal rate = COD removal efficiency × COD loading rate. Thus from the COD loading rate of 0.72 g day^{-1}, if the COD removal efficiency is x%, $I_{max.at}$ was calculated to be x% × 100.5 mA.

ATP measurement

The anodic electrode of an MFC of interest was taken out and washed with 100 mM phosphate buffered saline (PBS). A 0.2-mm-thick surface layer (including biomass) of a 1 cm^2 area of each electrode was scratched off and mixed with 1 ml of PBS. The mixture was subsequently vortexed vigorously to fragment the electrode particles before 50 ml of this mixture was allowed to react with 50 ml of an ATP measurement kit chemical (BacTiter-Glo Microbial Cell Viability Assay, Promega). After 5 min of reaction, the luminescence of this mixture was recorded. The ATP concentration of a sample was calculated from the luminescent intensity using an established standard ATP curve.

Molecular analysis

Total DNA of the aforementioned sample mixture was extracted using standard methods (Boon *et al.*, 2000). DNA was quantified based on UV absorption at 260 nm. 16S rRNA gene fragments were amplified with the primers PRBA338fGC and P518 (Muyzer *et al.*, 1993) and analysed using DGGE with a denaturing gradient ranging from 45% to 60% (Boon *et al.*, 2002). The fragments were also cloned into competent *Escherichia coli* TOP10 cells using TOPO TA cloning kits (Invitrogens); the clones obtained were used for sequencing the fragments. DNA sequencing was carried out by ITT Biotech Bioservice (Bielefeld, Germany). The analysis of DNA sequences and homology searches were completed with standard DNA sequencing programs and the BLAST server of the National Center for Biotechnology Information using the BLAST algorithm (Altschul *et al.*, 1997).

The CLSM

Anodic electrodes from the MFC enriched under high shear rates conditions (the high shear enriched MFC) and the MFC enriched under low shear rates conditions (the control or the low shear enriched MFC) were taken out and washed with 100 mM PBS. The electrodes were subsequently treated with cold methanol (–20°C) for 20 min to fix the bacterial cells.

After three times being rinsed with a $2 \times SSC$ solution (0.3 M NaCl, 0.03 M sodium citrate, pH 7.0) (each time for 1 min), they were incubated with a staining solution (1 mg ml^{-1} propidium iodine solution: $2 \times SSC$ solution = 1:3000 v/v) for 5 min to stain the DNA. Finally, the surfaces covered with biofilms of the electrodes were observed under confocal microscopy (Radiance, 2000 MP, Bio-Rad; mounted on a Nikkon Eclips 300 microscope) at the excitation wavelength of 488 nm. The images of biofilms were developed from fluorescent signals using ImageJ software. The structure of biofilms was analysed based on CLSM images using COMSTAT software (Heydorn *et al.*, 2000).

The SEM

Anodic electrodes from the high shear enriched MFC and the low shear enriched MFC were taken out and washed by 100 mM PBS. They were treated according to Park and colleagues (2001) to prepare samples for SEM observation. The treated samples were then coated with gold in a sputtering device (Baltec SCD005 Sputter Coater). A FEI XL30 ESEM with a LaB$_6$ filament was used to visualize the electrode surfaces.

Other analytical techniques

Electrical parameters were measured and calculated according to Aelterman and colleagues (2006) and Logan and colleagues (2006). Polarization curves were obtained according to Aelterman and colleagues (2006). Optical density of samples was measured using a UV and visible light spectrophotometer (Uvikon 932, Kontron Instruments). The COD measurements were done according to the dichromate method (Greenberg *et al.*, 1992). Any analysis or measurement, unless otherwise explained, was repeated three times.

References

Aelterman, P., Rabaey, K., Pham, H.T., Boon, N., and Verstraete, W. (2006) Continuous electricity generation at high voltages and currents using stacked microbial fuel cells. *Environ Sci Technol* **40:** 3388–3394.

Aelterman, P., Freguia, S., Keller, J., Verstraete, W., and Rabaey, K. (2008) The anode potential regulates bacterial activity in microbial fuel cells. *Appl Microbiol Biotechnol* **78:** 409–418.

Allen, R.M., and Bennetto, H.P. (1993) Microbial fuel cells – electricity production from carbohydrates. *Appl Biochem Biotechnol* **39:** 27–40.

Altschul, S.F., Madden, T.L., Schaffer, A.A., Zhang, J., Zhang, Z., Miller, W., and Lipman, D.J. (1997) Gapped BLAST and PSI-BLAST: a new generation of protein database search programs. *Nucleic Acids Res* **25:** 3389–3402.

Biffinger, J.C., Pietron, J., Ray, R., Little, B., and Ringeisen, B.R. (2007) A biofilm enhanced miniature microbial fuel cell using *Shewanella oneidensis* DSP10 and oxygen reduction cathodes. *Biosens Bioelectron* **22:** 1672–1679.

Bond, D.R., and Lovley, D.R. (2003) Electricity production by *Geobacter sulfurreducens* attached to electrodes. *Appl Environ Microbiol* **69:** 1548–1555.

Boon, N., Goris, J., De Vos, P., Verstraete, W., and Top, E.M. (2000) Bioaugmentation of activated sludge by an indigenous 3-chloroaniline degrading Comamonas testosteroni strain, I2gfp. *Appl Environ Microbiol* **66:** 2906–2913.

Boon, N., De Windt, W., Verstraete, W., and Top, E.M. (2002) Evaluation of nested PCR-DGGE (denaturing gradient gel electrophoresis) with group-specific 16S rRNA primers for the analysis of bacterial communities from different wastewater treatment plants. *FEMS Microbiol Ecol* **39:** 101–112.

Cao, Y.S., and Alaerts, G.J. (1995) Influence of reactor type and shear-stress on aerobic biofilm morphology, population and kinetics. *Water Res* **29:** 107–118.

Chang, I.S., Moon, H., Bretschger, O., Jang, J.K., Park, H.I., Nealson, K.H., and Kim, B.H. (2006) Electrochemically active bacteria (EAB) and mediator-less microbial fuel cells. *J Microbiol Biotechnol* **16:** 163–177.

Clauwaert, P., Rabaey, K., Aelterman, P., De Schamphelaire, L., Pham, T.H., Boeckx, P., *et al.* (2007) Biological denitrification in microbial fuel cells. *Environ Sci Technol* **41:** 3354–3360.

Dunsmore, B.C., Jacobsen, A., Hall-Stoodley, L., Bass, C.J., Lappin-Scott, H.M., and Stoodley, P. (2002) The influence of fluid shear on the structure and material properties of sulphate-reducing bacterial biofilms. *J Ind Microbiol Biotechnol* **29:** 347–353.

Gorby, Y.A., Yanina, S., McLean, J.S., Rosso, K.M., Moyles, D., Dohnalkova, A., *et al.* (2006) Electrically conductive bacterial nanowires produced by *Shewanella oneidensis* strain MR-1 and other microorganisms. *Proc Natl Acad Sci USA* **103:** 11358–11363.

Greenberg, A., Clesceri, L.S., and Eaton, A.D. (1992) *Standard Methods for the Examination of Water and Waste Water*, 18th edn. Washington, DC, USA: American public health association.

Heydorn, A., Nielsen, A.T., Hentzer, M., Sternberg, C., Givskov, M., Ersboll, B.K., and Molin, S. (2000) Quantification of biofilm structures by the novel computer program COMSTAT. *Microbiology-UK* **146:** 2395–2407.

Houtmeyers, J., Vandeneynde, E., Poffe, R., and Verachtert, H. (1980) Relations between substrate feeding pattern and development of filamentous bacteria in activated-sludge processes.1. Influence of process parameters. *Eur J Appl Microbiol Biotechnol* **9:** 63–77.

Kim, B.H., Kim, H.J., Hyun, M.S., and Park, D.H. (1999) Direct electrode reaction of Fe(III)-reducing bacterium, Shewanella putrefaciens. *J Microbiol Biotechnol* **9:** 127–131.

Kim, B.H., Park, H.S., Kim, H.J., Kim, G.T., Chang, I.S., Lee, J., and Phung, N.T. (2004) Enrichment of microbial community generating electricity using a fuel-cell-type electrochemical cell. *Appl Microbiol Biotechnol* **63:** 672–681.

Kim, J., Lee, C., Shin, S.G., and Hwang, S. (2008) Correlation of microbial mass with ATP and DNA concentrations in acidogenesis of whey permeate. *Biodegradation* **19:** 187–195. DOI 10.1007/s10532-007-9125-7.

Kucnerowicz, F., and Verstraete, W. (1979) Direct measurement of microbial ATP in activated-sludge samples. *J Chem Technol Biotechnol* **29:** 707–712.

Kugaprasatham, S., Nagaoka, H., and Ohgaki, S. (1992) Effect of turbulence on nitrifying biofilms at nonlimiting substrate conditions. *Water Res* **26:** 1629–1638.

Kwok, W.K., Picioreanu, C., Ong, S.L., van Loosdrecht, M.C.M., Ng, W.J., and Heijnen, J.J. (1998) Influence of biomass production and detachment forces on biofilm structures in a biofilm airlift suspension reactor. *Biotechnol Bioeng* **58:** 400–407.

Logan, B.E., and Regan, J.M. (2006) Electricity-producing bacterial communities in microbial fuel cells. *Trends Microbiol* **14:** 512–518.

Logan, B.E., Hamelers, B., Rozendal, R., Schrorder, U., Keller, J., Freguia, S., *et al.* (2006) Microbial fuel cells: methodology and technology. *Environ Sci Technol* **40:** 5181–5192.

van Loosdrecht, M.C.M., Heijnen, J.J., Eberl, H., Kreft, J., and Picioreanu, C. (2002) Mathematical modelling of biofilm structures. *Anton Leeuw Int J G* **81:** 245–256.

Marsili, E., Baron, D.B., Shikhare, I.D., Coursolle, D., Gralnick, J.A., and Bond, D.R. (2008) *Shewanella* Secretes flavins that mediate extracellular electron transfer. *PNAS* **105:** 3968–3973.

Massey, B.S. (1983) *Mechanics of Fluids*. 5th edn. Berkshire, UK: Van Nostrand Reinhold.

Muyzer, G., de Waal, E.C., and Uitterlinden, A. (1993) Profiling of complex microbial populations using denaturing gradient gel electrophoresis analysis of polymerase chain reaction-amplified genes coding for 16S rRNA. *Appl Environ Microbiol* **59:** 695–700.

Ohashi, A., and Harada, H. (1996) A novel concept for evaluation of biofilm adhesion strength by applying tensile force and shear force. *Water Sci Technol* **34:** 201–211.

Park, H.S., Kim, B.H., Kim, H.S., Kim, H.J., Kim, G.T., Kim, M., *et al.* (2001) A novel electrochemically active and Fe(III)-reducing bacterium phylogenetically related to *Clostridium butyricum* isolated from a microbial fuel cell. *Anaerobe* **7:** 297–306.

Pham, T.H., Rabaey, K., Aelterman, P., Clauwaert, P., De Schamphelaire, L., Boon, N., and Verstraete, W. (2006) Microbial fuel cells in relation to conventional anaerobic digestion technology. *Eng Life Sci* **6:** 285–292.

Pham, T.H., Boon, N., Aelterman, P., Clauwaert, P., De Schamphelaire, L., Vanhaecke, L., *et al.* (2008) Metabolites produced by *Pseudomonas* sp. enable a Gram-positive bacterium to achieve extracellular electron transfer. *Appl Microbiol Biotechnol* **77:** 1119–1129.

Picioreanu, C., van Loosdrecht, M.C.M., and Heijnen, J.J. (2001) Two-dimensional model of biofilm detachment caused by internal stress from liquid flow. *Biotechnol Bioeng* **72:** 205–218.

Rabaey, K., and Verstraete, W. (2005) Microbial fuel cells: novel biotechnology for energy generation. *Trends Biotechnol* **23:** 291–298.

Rabaey, K., Ossieur, W., Verhaege, M., and Verstraete, W. (2005) Continuous microbial fuel cells convert carbohydrates to electricity. *Water Sci Technol* **52:** 515–523.

Rabaey, K., Rodriguez, J., Blackall, L.L., Keller, J., Gross, P., Batstone, D., *et al.* (2007) Microbial ecology meets electrochemistry: electricity-driven and driving communities. *ISME J* **1:** 9–18.

Reguera, G., McCarthy, K.D., Mehta, T., Nicoll, J.S., Tuominen, M.T., and Lovley, D.R. (2005) Extracellular electron transfer via microbial nanowires. *Nature* **435:** 1098–1101.

Reguera, G., Nevin, K.P., Nicoll, J.S., Covalla, S.F., Woodard, T.L., and Lovley, D.R. (2006) Biofilm and nanowire production leads to increased current in *Geobacter sulfurreducens* fuel cells. *Appl Environ Microbiol* **72:** 7345–7348.

Wilkinson, S. (2000) 'Gastrobots' – benefits and challenges of microbial fuel cells in food powered robot applications. *Auton Robots* **9:** 99–111.